Spontaneous fluctuations in free-molecular flow:

theory, simulations, and preliminary experiments

Dawson M. Willerton

Department of Physics

McGill University

Montréal, Québec, Canada

August 2023

A thesis submitted to McGill University in partial fulfillment of the requirements for the degree of Master of Science.

Acknowledgements

Firstly, I would like to thank Walter Reisner and Guillaume Gervais for the opportunities that they have given me. To Guillaume in particular, who has been the impetus behind so much of what I have done and how I have improved during my studies, thank you for welcoming me so warmly and accommodatingly into the wonderful group of scientists that you have cultivated at McGill. The work that I have done over these past two years, and have here compiled into this document, would not have been possible without the help and encouragement of the community of people that constitute GervaisLab. Specifically, I would like to highlight my gratitude toward Nick Wicklund for the numerous roles that he has played to these effects, both as a friend and as a lab partner, and toward Jehan Dastoor for initializing me on my first arriving in Montréal. Additionally, I thank Frederik Poitevin for helping with far too many things to count inside of the lab, and Zachary Berkson-Korenberg for his *world-class* tech support and for helping me to optimize my simulations. A special thank you to other members of the lab who have repeatedly made themselves available to answer questions and to help where needed, and who have each played a vital role in keeping its atmosphere as pleasant and as lively as I have experienced it to be – thank you to Sujatha Vijayakrishnan, Matei Petrescu, Talia Martz-Oberlander, and Oulin Yu. The effect of working among such a vibrant community of smart and productive people I think cannot be overstated, thus I reiterate once more the immense debt of gratitude that I owe to the *whole* of GervaisLab – thank you all.

I would also like to thank Robert Gagnon, Richard Talbot, and John Smeros for the innumerable ways in which they have contributed to keeping GervaisLab functional. Thank you also to Jean-Philippe Massé of $(CM)^2$ at Polytechnique Montréal for his thorough assistance in fabricating our nanopores, and to Pascal Bourseguin and Marc Giroux of the McGill machine shop for building us various experimental components.

Finally, I wish to thank my friends and family back in Oshawa. In particular, thank you to my brother, Brandon, for so many things that I make no attempt to capture them here. Thank you also to my sister Samantha for acting as a beacon of positivity and inspiration; and to my parents, Kelly and Andrew, for the unique roles that they have each played in leading me to where I am today.

Abstract

This thesis extends principles from past analyses of innate fluctuations in electrical circuits to the study of a simple class of free-molecular fluidic systems on the basis of an apparent analogy. This is primarily done through a derivation that draws from past electrical work to propose a measure of the limiting noise that exists in gas flow across pores when particle-particle collisions are assumed to be negligible. The results obtained from theory are then reiterated with the use of a basic Monte Carlo program that has been rigged to simulate a fluctuating average flow signal, thus permitting the estimation of a simulated mass-flow noise power in addition to transmission probabilities for a variety of pore geometries. The beginning of an experimental investigation seeking to confirm the mass-flow fluctuations expected from theory and simulation is also documented. Although no definitive conclusions in this respect are made, the experimental setup is characterized in various respects and some possible directions for future work are briefly discussed.

Abrégé

Cette thèse étend quelques principes des études précédentes sur les fluctuations inhérentes dans les circuits électriques à celle d'une classe simple de systèmes fluidiques analogues. Principalement, cela est réalisé par une dérivation s'inspirant de la théorie des circuits électriques afin de proposer une expression pour le bruit limitant dans le transport de gaz à travers les nanopores quand les collisions entre des particule sont négligeables. Les résultats obtenus à partir de la théorie sont ensuite reproduits à l'aide d'un programme de type Monte Carlo qui a été adapté pour simuler un signal moyen fluctuant. Cela permet ainsi l'estimer à la fois la puissance de bruit simulée et les probabilités de transmission une variété pores ayant différentes géométries. Quelques premières étapes expérimentales visant à valider les résultats issus de la théorie et des simulations sont aussi présentées. Bien qu'une conclusion définitive à cet égard n'est pas atteinte, le montage expérimental est caractérisé et quelques directions possibles pour les travaux futurs sont explorées.

Contributions

The initial idea behind the investigations presented in this thesis is credited to Guillaume Gervais and Walter Reisner. The simulation and theory work presented in Chapter 2 was carried out by the author of this thesis and builds off of work done by and in collaboration with previous members of GervaisLab, namely Daniel Crook (test-particle simulation method) and Jehan Dastoor (mass-flow noise theory) respectively.

Most of the data collection involved in Chapter 3 was also carried out by the author, however undergraduate student Julien Hacot-Slonosky and Nick Wicklund made contributions as well. Additionally, the majority of the technical work involved in putting together the experimental setup was done in collaboration with Nick Wicklund. Jehan Dastoor also played a significant role in this respect, and many of the experimental components and procedures used by past members of the lab were recycled, particularly in so far as they pertained to the handling of gas flow in our measurement system. Specifically, the past works of graduate students Pierre-François Duc, Michel Savard, Sam Neale, and Guillaume Dauphinais were crucial to establishing our experimental method.

Contents

List of figures

List of tables

Chapter 1

Introduction

The study of fluctuations in physical systems is of crucial importance to many areas of science and of technology [1]. In cultivating an understanding of the irregular behaviours that underlie our well-behaved macroscopic pictures, we are often led to deeper insights into the systems of our studies. In many cases, such a resolution of understanding lends itself to some practical consequence. For instance, in sensitive measurement apparatuses for which the signal of interest is very small, experiments often must be carefully navigated around a background of fluctuations in order for data to be reliably collected and interpreted. Additionally, statistical measures of physical fluctuations are often predictable as expressions of certain properties of the system and thus may constitute a signal of interest in themselves.

Perhaps among the most well-known examples of fluctuations in physical systems is the so-called *Johnson-Nyquist (thermal) noise* of electrical resistors [2, 3]. Formulated in terms of mean-square current fluctuations, the Johnson-Nyquist noise expected to be observed in resistors for a measurement bandwidth Δf is given by

$$\langle (\delta I_{Thermal})^2 \rangle = 4 k_B T R^{-1} \Delta f, \tag{1.1}$$

and has its origin in the fact that electrons in resistors are free to bounce around with random velocities, in accordance with their innate thermal motions. In this way, a fluctuating current

signal may form across resistors even in the absence of an applied voltage.

Another kind of fluctuations present in electrical systems is the *electrical shot noise* which was first discovered by Walter Schottky in vacuum tube diodes [4]. In such simple systems, the electrical shot noise takes the form

$$\langle (\delta I_{Shot})^2 \rangle = 2e \langle I \rangle \Delta f, \tag{1.2}$$

which is proportional to the average current across the diode, $\langle I \rangle$. This kind of noise may be likened to the pitter-patter of a light rain in the sense that the current signal I is actually comprised of a stream of discrete charge carriers which arrive irregularly on the surface of the current detector, giving rise to an analogous pitter-patter effect.

In this thesis, our focus will be on studying fluctuations in the rate of mass flowing across nanopores[1] inside of the so-called *free-molecular flow regime*. In part, we are motivated by the fact that the behaviour of fluids confined in nanopores is a subject of broad research interest, in physics and especially in biological applications [5–8], and thus an understanding of the fluctuations present in such systems may in various ways be beneficial to future research and technological pursuits. Additionally, we are motivated by an analogy between mass-flow circuits and electrical circuits in the following two respects:

1. A pore in a (pressure-driven) mass flow circuit behaves similarly to an electrical resistor in an electrical circuit in the linear regime, and indeed may be characterized by an analogue of Ohm's law:

$$\langle I \rangle = R^{-1} \Delta V \longleftrightarrow \langle Q \rangle = G \Delta P.$$

2. The mass-flow current Q may be understood as a consisting in a stream of discrete

[1] Here and throughout, we use the term "nanopore" somewhat loosely — the conditions of our analysis do not inherently confine us to the nanoscale, though it is entailed for most real systems.

mass carriers, *i.e.* the fluid particles, much like how the electrical current I may be understood as consisting in a stream of discrete charge carriers:

$$e \longleftrightarrow m.$$

Explicitly, on the basis of this described analogy with electrical circuits, we might expect to see similar species of physical fluctuations in mass-flow systems to those reflected in Equation 1.1 and Equation 1.2. Indeed, it is the aim of this thesis to pursue further and to characterize these suspected mass-flow fluctuations.

Chapter 2

Theory and simulation

2.1 Basic concepts in the theory of random processes

Before setting out on our investigation into mass-flow fluctuations, it will be prudent to survey some elementary concepts from the theory of random processes. This we do with the aim of equipping ourselves to speak the appropriate language for dealing with physical fluctuations broadly, and in free-molecular fluidic systems particularly.

2.1.1 Stochastic processes

A central object in probability theory is the *random variable*, which is typically denoted X and defined in association with its corresponding *sample space* S_X [9]. If we consider, for instance, the simple case of rolling a single die, then we may define a discrete random variable to be the number displayed on the top face of the die after it has been rolled. The sample space of our die-rolling experiment refers to the possible values[1] that may be inherited by X upon what we might call measurement – of course, for an ordinary six-sided die, these are

[1]Formally, the values are provided by a map that takes members of the sample space (which denotes the possible *observations* in a random experiment) to a number assignment for X. For our purposes, the random variable *is* the observation, and thus the distinction between the so-called *range* of X and its sample space is not important. This standard persists in subsequent sections.

just the values contained in the set $S_X = \{1, 2, 3, 4, 5, 6\}$.

The *probability mass function* $f(X)$ provides a mapping between the values contained in S_X and, speaking loosely, the plausibility of their being identified in a given instance of X. If we suppose that our die is fair, then in our case this probability mass function is simply $f(X) = 1/6$ for all $X \in S_X$ and zero otherwise. The mean, the variance, and other such familiar statistical quantities associated with X may be found by interrogation of $f(X)$ in the ordinary ways.

The *random* (or *stochastic*) *process* may be regarded as the natural extension of the random variable into the time domain [10]. As such, many of the above-mentioned concepts from the probability theory of random variables will be found also to apply in our study of stochastic processes, with the main difference being that – in shifting our focus from *variables* to *processes* – the object of interest becomes $X(t)$, which is seen to be a function of time. The sample space correspondingly now consists in the set of functions $S_{X(t)} = \{x_1(t), x_2(t), x_3(t), ..., x_N(t)\}$, which denote the realizable instances of $X(t)$ that may be observed during a single experiment.

2.1.2 Properties of stochastic processes

A random process $X(t)$ is permitted to be either continuous or discrete in both its range and domain. Thus, in analogy to the discrete-continuous dichotomy of random variables, there exist four basic categories of stochastic processes which are summarized in Table 2.1 below [11].

Random processes may also be characterized by statistical quantities such as the mean and the variance. It must be noted, however, that there is a subtlety in taking averages of a stochastic process, which is that we are afforded two choices: we may choose to average over time or over the ensemble of sample functions [12]. For instance, in the case of a c.d. stochastic process, we have the option of computing

	Continuous t	Discrete t
Continuous $X(t)$	Continuous-time, continuous-value (c.c.)	Discrete-time, continuous-value (d.c.)
Discrete $X(t)$	Continuous-time, discrete-value (c.d.)	Discrete-time, discrete-value (d.d.)

Table 2.1: The four basic classifications of stochastic processes. These names will henceforth be abbreviated under the convention shown in parentheses.

$$\langle x_i(t) \rangle = \frac{1}{T} \int_{-T/2}^{T/2} x_i(t) dt \tag{2.1}$$

to obtain the *time-averaged* mean of an observed instance of $X(t)$, *i.e.* $x_i(t)$, as it appears over the measurement interval $t \in [-T/2, T/2]$. We may otherwise choose to compute

$$\bar{X}(t_j) = \frac{1}{N} \sum_{i}^{N} x_i(t_j),$$

to obtain the *ensemble-averaged* mean of $X(t)$ at a particular time t_j. The concept behind each procedure is depicted in Figure 2.1 and the freedom applies equally well to computations of other averages such as the variance.

Throughout this thesis, we will be dealing with stochastic processes that are said to be *ergodic*, which means that the two averaging procedures described above are expected to yield the same values so long as the time average is done over a sufficiently long period [10]. This is a reasonable assumption to make for many physical systems and will indeed apply to all model processes used in this thesis.

In addition, all of the processes we will encounter in this thesis are *stationary*, which may be understood to imply that $X(t)$, for all instants of time, may be regarded as a time-indexed collection of Xs drawn from a constant probability mass (or density) function $f(X)$. We also note that another implication of stationarity in this sense is that quantities such as the mean, the variance, and other expectation values are all guaranteed to be constant as well.

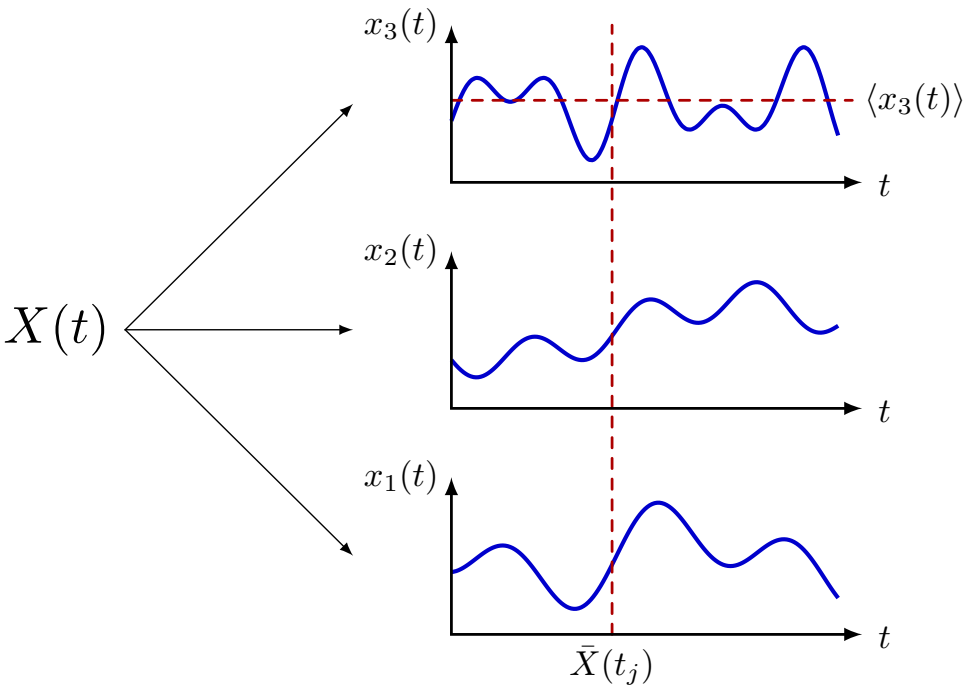

Figure 2.1: Illustration of the two methods for taking averages of stochastic processes. The arrows on the left point to possible realizations of $X(t)$ over a single experiment, *i.e.* to the functions $x_i(t)$ which comprise the sample space $S_{X(t)}$. For simplicity, we have supposed that this sample space consists of only three functions, and thus the ensemble average $\bar{X}(t_j)$ is seen to be computed over all of the sample functions as they appear at a particular point in time t_j.

2.1.3 Autocorrelation and the power spectral density

A more sophisticated means of characterizing a random process is by determination of its (one-sided[2]) *power spectral density* $S_X(f)$. In order to better appreciate what this quantity means, it is helpful to first explain the concept of the *autocorrelation function* and how it relates to the former.

In the context of stochastic processes, the autocorrelation function loosely refers to the degree of coherence with which $X(t)$ progresses in time. If we consider the value of $X(t)$ at each instant in time as constituting a random variable, then the autocorrelation function is

[2]For real physical processes, negative frequencies are redundant and it is therefore practical to compute one-sided power spectra. The two-sided spectrum is always symmetric for a stationary process and thus any $S_X(f)$ encountered in this thesis will be twice as large as its associated two-sided density.

related to the covariance of the two random variables $X(t)$ and $X(t+\tau)$; it functions as a measure of how much the value of $X(t)$ is expected to retain over a period of time τ.

Formally, the autocorrelation function of $X(t)$ over the period τ is defined as

$$R_X(t,\tau) = E[X(t)X(t+\tau)], \tag{2.2}$$

where $E[...]$ denotes an expected value [11]. As mentioned above, our concern throughout this thesis is with stationary stochastic processes, for which the associated $R_X(t,\tau)$ functions are expected to depend only on the elapsed time τ, *i.e.* we will be dealing with autocorrelation functions of the type

$$R_X(t,\tau) = R_X(\tau). \tag{2.3}$$

The utility of the autocorrelation function in studying stochastic processes exists largely in its relation to calculating power spectral densities. Explicitly, the passage from $R_X(\tau)$ to $S_X(f)$ is done by means of a Fourier transform via the *Wiener-Khintchine theorem*:

$$S_X(f) = 2\int_{-\infty}^{\infty} R_X(\tau)e^{i2\pi f\tau}d\tau, \tag{2.4}$$

for $f \in \mathbb{R}$ and $S_X(f) = 0$ otherwise. We note that $S_X(f)$ and $R_X(\tau)$ are thus seen to be two equivalent means of characterizing the time structure of $X(t)$.

Conceptually, while the autocorrelation function gives a measure of the extent to which a random process is expected to depart from its present value over some period of time, the power spectral density may be thought of as capturing the spectral character with which these departures take place.

Equivalently, we may choose to regard $S_X(f)$ as an expression of the random signal in terms of its frequency contents, which is more clearly seen when it is written as

$$S_X(f) = \lim_{T\to\infty}\frac{2}{T}E\left[\left|\int_{-T/2}^{T/2} X(t)e^{-i2\pi ft}dt\right|^2\right], \tag{2.5}$$

where the result of the integration has units of $[X^2(t)/f]$, *i.e.* $S_X(f)$ is seen to be a linear power[3] density along frequency. We reiterate that Equation 2.5 is defining a *one-sided* power spectral density, meaning that $S_X(f)$, as encountered above, takes only positive frequencies as inputs and otherwise goes to zero. Note that Equation 2.5 is clearly reminiscent of the Fourier transform and in particular may be thought of as analogous to the decomposition of a function into its Fourier components [12].

2.1.4 The Poisson process

The *Poisson process* is a simple example of a c.d. stochastic process that plays a crucial role in our modelling of mass flow in the free-molecular flow regime [10].

A stochastic process $N(t)$ is firstly said to be a *counting process* if its sample functions are everywhere non-decreasing and each obey

$$n_i(t) \in \mathbb{Z}^+ \text{ for all } t. \tag{2.6}$$

The value of $N(t)$ may therefore be interpreted as a positive integer count of some abstract sense of *arrivals*, or occurrences.

$N(t)$ is additionally said to be a Poisson process of rate parameter λ if it has the following properties:

1. The number of arrivals over any time interval of duration τ is a *Poisson variable* with a mean of $\lambda\tau$.

2. For any two non-overlapping time intervals $(t, t+\tau]$ and $(t', t'+\tau']$, the associated random variables $N(t+\tau)-N(t)$ and $N(t'+\tau')-N(t')$ are independent of each other.

In the first property listed above, we have invoked the ordinary Poisson random variable,

[3] Here we use "power" in the signal-processing sense, implying units of [signal^2].

which in this case is implied to have the probability mass function

$$f(N_\tau) = \frac{(\lambda\tau)^{N_\tau}}{N_\tau!} e^{-\lambda\tau}, \tag{2.7}$$

with N_τ referring to the number of arrivals accumulated over the period τ. We note that in order for Poisson statistics to apply, λ must be constant in time and all arrivals must happen independently, *i.e.* without influencing any other arrivals.

We may also note that the probability density function associated with the *wait times* between events t_w, which is the time elapsed between two successive arrivals, is given by

$$f(t_w) = \lambda e^{-\lambda t_w}. \tag{2.8}$$

2.1.5 The Nyquist-Shannon sampling theorem

Finally, before proceeding onto our discussion of mass-flow fluctuations, we make a brief note on the act of sampling a random process that is relevant to characterizing spectral densities experimentally.

As an example, we consider the case of measuring the instantaneous current $I(t)$ passing through a resistor in an electrical circuit. If we use an ideal ammeter that reports measurements at a fixed rate f_s then the result of our observation is a sequence of values that are separated in time by a fixed period $1/f_s$. In other words, the result of our measurement is a d.c. stochastic process that represents an incomplete image of the underlying c.c. fluctuating current, as shown in Figure 2.2.

It is thus clear that we are destined to miss some of the current signal in any attempt at measuring it with finite f_s and a crucial question thus arises: given a sequence of samples of a random process, what are we permitted to infer about the time structure of the underlying signal? The *Nyquist-Shannon sampling theorem* tells us that our selection of f_s places an upper bound on the frequency band over which we can reliably estimate the power spectral

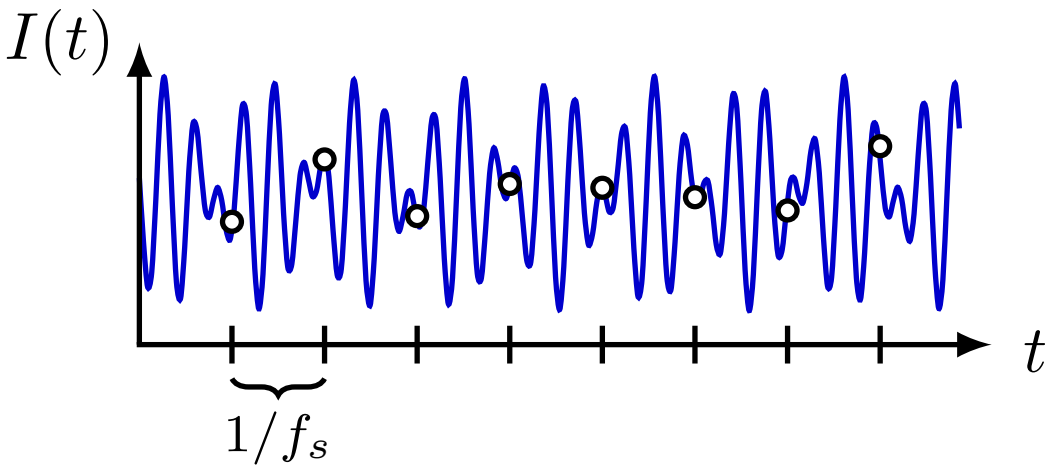

Figure 2.2: Cartoon of a continuous, fluctuating current signal (c.c. process) that is sampled at a fixed sampling rate f_s. The samples, plotted with black circles filled white, are seen to be evenly spaced by intervals of $1/f_s$ and thus constitute a related, but not identical, fluctuating current signal that is not continuous in time (d.c. process).

density of the underlying process [11]. Explicitly, the theorem says that given a sampling rate f_s, the frequency contents of the true signal may only be accurately determined over the frequencies $f \in [0, f_s/2]$[4]. Put in other words, the theorem tells us that in order to successfully reconstruct a component of a signal that oscillates with some definite frequency f_0, it must be sampled at a rate no less than $2f_0$.

[4]Here our convention of speaking in terms of one-sided spectral densities persists.

2.2 Theory of mass-flow fluctuations in the free-molecular flow regime

Now that we have been properly armed with some basic terminology from the theory of stochastic processes, we turn our attention to the study of mass-flow fluctuations in the free-molecular flow regime. In this section, we will discuss mass flow in nanopores and develop an idealized model of free-molecular flow as a stochastic process. We then derive the power spectral density associated with mass-flow fluctuations as a proposed measure of the limiting noise inherent in the free-molecular flow regime. Finally, we take note of some complications that are neglected in our model but may be relevant for future work.

2.2.1 Description of mass flow in nanopores

We begin by giving a detailed account of the class of systems that we are here concerned with. Suppose that we have a nanopore of diameter D and length L that connects two otherwise isolated reservoirs, which we label A and B. In addition, we suppose that each reservoir contains a volume of an inert gas at a constant temperature T and is maintained at some fixed pressure such that P_A and P_B are constant but not necessarily equal. The essence of the system that we have described is illustrated in Figure 2.3.

In addition, it will be useful to characterize the pore in our system by its *mass conductance* G, as defined by the equation

$$G = \frac{\langle Q(t) \rangle}{\Delta P} \tag{2.9}$$

where $Q(t)$ is the net rate of mass flow across the pore with units of [mass/time] and ΔP is the pressure differential between the reservoirs. It may be seen that G has standard units of m·s and we reiterate that it plays an analogous role in mass-flow circuits to that of the conductance of resistors in electrical circuits.

In further identifying our system, it will be helpful to appeal to a quantity called the

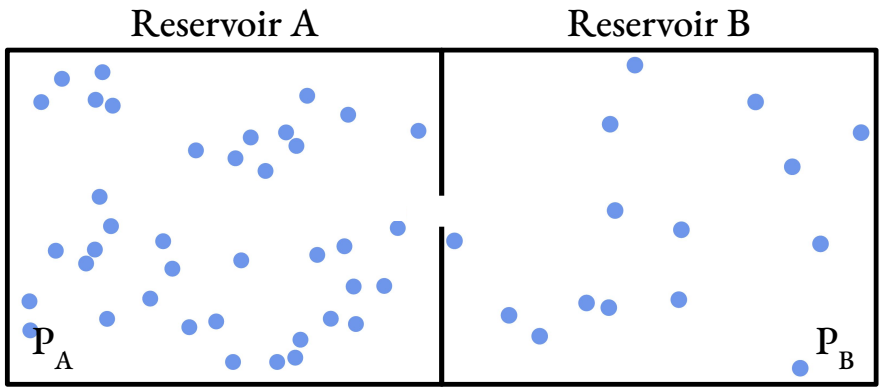

Figure 2.3: Two reservoirs containing a dilute gas are connected by a nanopore. The entire system is supposed to be in thermal equilibrium, though a pressure differential across the pore may exist. Furthermore, the reservoirs are imagined to be sufficiently large (or otherwise to have some regulatory pumping system) so as to ensure that the pressures P_A and P_B are constant.

Knudsen number, defined

$$\mathrm{Kn} \equiv \lambda / D, \tag{2.10}$$

where λ refers to the mean free path of the flowing gas[5]. The Knudsen number signifies the dominant scattering mechanism for particles as they travel through the pore and is therefore a suitable foundation for defining a spectrum of *flow regimes*, as shown in Figure 2.4. The utility of Kn is thus in serving as an approximate indicator for what treatment is appropriate for modelling gas flow in our system – it loosely tells us what sort of physics is expected to go into determining G in Equation 2.9.

Throughout the rest of this thesis, we confine our analysis to the *free-molecular* flow regime, *i.e.* to systems that are characterized by $\mathrm{Kn} > 10$. Physically, this means that we will be dealing with systems of dilute gases for which interparticle collisions are negligible and we find ourselves outside the domain of applicability for the Navier–Stokes equations which describe the dynamics of a fluid that has been modeled as a continuum. Our focus is

[5]Of course, in our system there are actually two mean free paths – one for each reservoir. This will not be a crucial point for our purposes, but we could substitute λ with an appropriately-weighted average of λ_A and λ_B if we wanted to be more stringent.

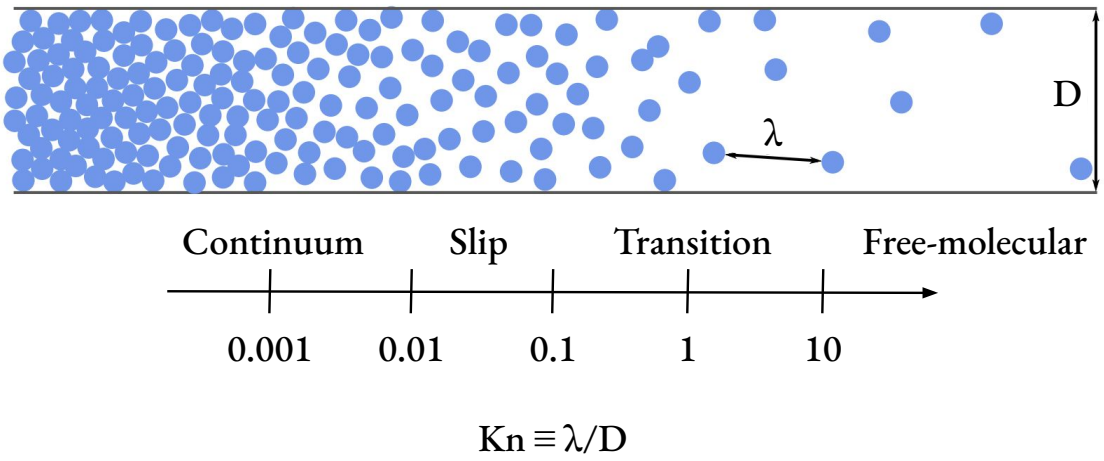

Figure 2.4: Typical classification of gas flow regimes based on the Knudsen number (Kn). Figure adapted from [13].

thus turned to developing a picture of trans-pore flow in terms of individual particles, their trajectories, and, en masse, their statistics.

2.2.2 Free-molecular flow as a stochastic process

We now consider the rate of particle arrivals at either entrance of our pore. Since the gas in our system is modelled as dilute and inert, we will be justified in treating it as ideal. From statistical mechanics, the particle flux on the walls of a container holding an ideal gas is

$$\Phi = \frac{1}{4} n \bar{v}, \tag{2.11}$$

where $\bar{v}$ is the average speed of the gas particles. The rate of particles reaching either entrance of the pore is thus obtained by multiplying the flux in Equation 2.11 with the cross-sectional

area of the pore, yielding

$$\begin{aligned}\langle r(t)\rangle &= \Phi A \\ &= \frac{1}{4}\left(\frac{P}{k_B T}\right)\left(\sqrt{\frac{8k_B T}{\pi m}}\right)\left(\frac{\pi D^2}{4}\right) \\ &= \frac{1}{4}\sqrt{\frac{\pi}{2mk_B T}}D^2 P,\end{aligned} \tag{2.12}$$

where we have made the appropriate substitutions for n and $\bar{v}$. It is clear from Equation 2.12 that we will have to distinguish between $r_A(t)$ and $r_B(t)$ since the reservoir pressures are generally not the same[6]. We may also define the rates of transfer between reservoirs such that the mean rates are given by

$$\langle r_{A\to B}(t)\rangle = \kappa_{A\to B}\langle r_A(t)\rangle\,, \tag{2.13}$$

and

$$\langle r_{B\to A}(t)\rangle = \kappa_{B\to A}\langle r_B(t)\rangle\,, \tag{2.14}$$

where we have introduced *Clausing factors*, denoted $\kappa_{A\to B}$ and $\kappa_{B\to A}$. We can interpret each Clausing factor as the probability that an incident particle will successfully pass through the pore in the specified direction – with $1-\kappa$ being the probability that the particle is instead reflected back to its original reservoir. For the sake of brevity, we will assume a pore geometry such that $\kappa_{A\to B} = \kappa_{B\to A}$, but this is an assumption that is easily relaxed[7].

Since we have confined ourselves to the free-molecular flow regime, individual particles are expected to travel across the pore without any influence from other particles. This, in combination with the fact that we have decided to hold all pressures and temperatures

[6]The diameters may also be different, depending on the geometry of the pore. Here we make the assumption that this is not the case, but we could straightforwardly accommodate asymmetries of this kind by distinguishing two direction-specific nanopore conductances $G_{A\to B}$ and $G_{B\to A}$.

[7]Prescription from the previous footnote applies here as well.

constant, implies that Equations 2.13 and 2.14 may be regarded as specifying rate parameters for two separate Poisson processes. Namely, we can establish the quantities $N_{A\to B}(t)$ and $N_{B\to A}(t)$ as integer counts of the particles that have passed between reservoirs in the specified ways.

It is also helpful to establish the convention that the pressures of the reservoirs may be decomposed into

$$P_A = \Delta P + P_0 \text{ and } P_B = P_0, \tag{2.15}$$

such that reservoir A is taken to be the region of higher pressure, if one exists (*i.e.* with $\Delta P \geq 0$), and reservoir B is used to mark a baseline pressure P_0. Additionally, we may choose to define the *net* particles that have passed through the pore in the direction of A to B[8] as

$$\mathbf{N}(t) \equiv N_{A\to B}(t) - N_{B\to A}(t), \tag{2.16}$$

where it may be seen that a negative $\mathbf{N}(t)$ corresponds to a net passage of particles in the direction of B to A. Note that despite our using notation similar to that used in defining counting processes in the previous section, the sample functions of $\mathbf{N}(t)$ are permitted to decrease and do not necessarily satisfy Equation 2.6. This means that the net process $\mathbf{N}(t)$ cannot generally be considered a counting process and thus, *a fortiori*, neither can it generally be considered a Poisson process[9].

The instantaneous rate of change in $\mathbf{N}(t)$ with respect to time may be understood as a measure of the instantaneous particle flow rate in our system, and is thus crucial for our investigation. We may identify the time derivative of $\mathbf{N}(t)$ with the random process

$$\mathbf{r}(t) = r_{A\to B}(t) - r_{B\to A}(t), \tag{2.17}$$

[8]This is analogous to setting the convention that electrical current flows in the direction that positive charges move.

[9]It would formally be called a *Skellam process*.

such that

$$\mathbf{N}_\tau = \int_0^\tau \mathbf{r}(t)dt \tag{2.18}$$

is the value accumulated by $\mathbf{N}(t)$ over a period of duration τ[10]. The function $\mathbf{r}(t)$ may be idealized as consisting in a sequence of Dirac delta functions, *i.e.*

$$\mathbf{r}(t) = \sum_a \delta(t - t_a) - \sum_b \delta(t - t_b), \tag{2.19}$$

with a and b indexing the pulse times corresponding to particles originating in reservoirs A and B respectively. The relationship between $\mathbf{r}(t)$ and $\mathbf{N}(t)$ is illustrated in Figure 2.5.

Having now established the basic infrastructure for modelling free-molecular flow through nanopores as a stochastic process, we are equipped to embark on a derivation of the mass-flow fluctuations.

[10]We lose no generality in starting the bounds of integration at $t = 0$. This is because $\mathbf{N}(t)$ is composed of two Poisson processes and thus inherits the property that the distribution of arrivals in a given time interval depends only on its length.

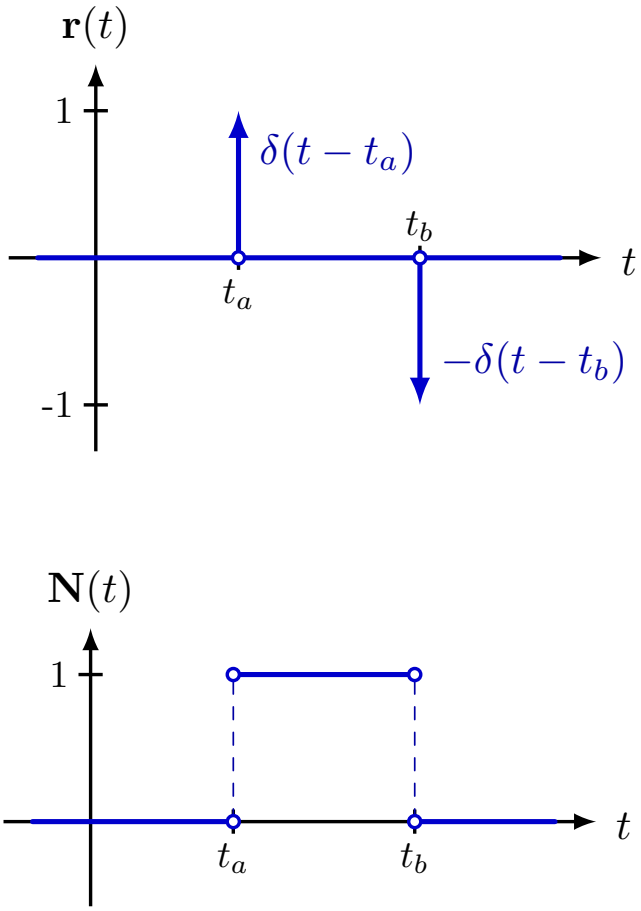

Figure 2.5: Conceptual plots of the processes $\mathbf{r}(t)$ and $\mathbf{N}(t)$. The passage from a realization of $\mathbf{r}(t)$ to the corresponding realization of $\mathbf{N}(t)$ is seen to be done via integration over a series of Dirac delta functions, leading to a step function that has the option of stepping up or down by 1 unit at a time.

2.2.3 Mass-flow fluctuations

Our strategy here is to begin with an analysis of fluctuations in the rate of particle flow across our pore and to then translate these results into a measure appropriate for mass-flow fluctuations. As such, we firstly consider the instantaneous fluctuations in $\mathbf{r}(t)$, defined as

$$\delta\mathbf{r}(t) \equiv \mathbf{r}(t) - \langle \mathbf{r}(t) \rangle \,, \tag{2.20}$$

such that the mean square fluctuation is given by

$$\begin{aligned}\langle(\delta\mathbf{r}(t))^2\rangle &= \langle(\mathbf{r}(t) - \langle\mathbf{r}(t)\rangle)^2\rangle \\ &= \langle\mathbf{r}^2(t)\rangle - \langle\mathbf{r}(t)\rangle^2\end{aligned}$$

and represents the total power of the fluctuations delivered to $\mathbf{r}(t)$. If such fluctuations are deemed irrelevant to the signal of interest, say for instance to the quantity $\langle\mathbf{r}(\mathbf{t})\rangle$, and are in this sense considered to play some destructive role during measurements, then this value also serves as a measure of the total *noise power* contained in the signal.

Since we would like to characterize the time structure of these fluctuations in terms of their associated power spectrum, we seek first to compute the associated autocorrelation function. The autocorrelation function for the fluctuations in $\mathbf{r}(t)$ may be written as

$$\begin{aligned}E[\delta\mathbf{r}(t)\delta\mathbf{r}(t+\tau)] &= \langle\delta\mathbf{r}(t)\delta\mathbf{r}(t+\tau)\rangle \\ &= \langle\mathbf{r}(t)\mathbf{r}(t+\tau)\rangle - \langle\mathbf{r}(t)\rangle\langle\mathbf{r}(t) + \mathbf{r}(t+\tau))\rangle + \langle\mathbf{r}(t)\rangle^2 \\ &= \langle\mathbf{r}(t)\mathbf{r}(t+\tau)\rangle - \langle\mathbf{r}(t)\rangle^2 . \qquad (2.21)\end{aligned}$$

The second term on the last line of Equation 2.21 is essentially known already[11], so we will focus on computing the first. Following the method used in Ref. [14], we begin by expanding

[11] The mean of $\mathbf{r}(t)$ may be found straightforwardly from its definition in Equation 2.17.

$\mathbf{r}(t)$ and $\mathbf{r}(t+\tau)$ as sums of randomly distributed Dirac delta functions via Equation 2.19:

$$\begin{aligned}\langle \mathbf{r}(t)\mathbf{r}(t+\tau)\rangle &= \Big\langle \Big(\sum_a \delta(t-t_a) - \sum_b \delta(t-t_b)\Big)\Big(\sum_{a'} \delta(t+\tau-t_{a'}) - \sum_{b'} \delta(t+\tau-t_{b'})\Big)\Big\rangle \\ &= \Big\langle \sum_{a,a'} \delta(t-t_a)\delta(t+\tau-t_{a'}) - \sum_{a,b} \delta(t-t_a)\delta(t+\tau-t_b) \\ &\qquad - \sum_{b,a} \delta(t-t_b)\delta(t+\tau-t_a) + \sum_{b,b'} \delta(t-t_b)\delta(t+\tau-t_{b'})\Big\rangle. \quad (2.22)\end{aligned}$$

At this point, it is helpful to isolate the correlated pulses from the uncorrelated pulses by splitting the relevant sums. In doing so, we end up with

$$\begin{aligned}\langle \mathbf{r}(t)\mathbf{r}(t+\tau)\rangle &= \Big\langle \sum_a \delta(t-t_a)\delta(t+\tau-t_a)\Big\rangle + \Big\langle \sum_{a\neq a'} \delta(t-t_a)\delta(t+\tau-t_{a'})\Big\rangle \\ &\qquad - \Big\langle \sum_{a,b} \delta(t-t_a)\delta(t+\tau-t_b)\Big\rangle - \Big\langle \sum_{b,a} \delta(t-t_b)\delta(t+\tau-t_a)\Big\rangle \\ &\qquad + \Big\langle \sum_{b\neq b'} \delta(t-t_b)\delta(t+\tau-t_{b'})\Big\rangle + \Big\langle \sum_b \delta(t-t_b)\delta(t+\tau-t_b)\Big\rangle, \quad (2.23)\end{aligned}$$

where it may be noted that t_a, $t_{a'}$, t_b, and $t_{b'}$ are now completely uncorrelated and we may thus write

$$\begin{aligned}\langle \mathbf{r}(t)\mathbf{r}(t+\tau)\rangle &= \Big\langle \sum_a \delta(t-t_a)\delta(t+\tau-t_a)\Big\rangle + \Big\langle \sum_a \delta(t-t_a)\Big\rangle\Big\langle \sum_a \delta(t+\tau-t_a)\Big\rangle \\ &\qquad - \Big\langle \sum_a \delta(t-t_a)\Big\rangle\Big\langle \sum_b \delta(t+\tau-t_b)\Big\rangle - \Big\langle \sum_b \delta(t-t_b)\Big\rangle\Big\langle \sum_a \delta(t+\tau-t_a)\Big\rangle \\ &\qquad + \Big\langle \sum_b \delta(t-t_b)\Big\rangle\Big\langle \sum_b \delta(t+\tau-t_b)\Big\rangle + \Big\langle \sum_b \delta(t-t_b)\delta(t+\tau-t_b)\Big\rangle, \\ &\qquad\qquad (2.24)\end{aligned}$$

since $E[XY] = E[X]E[Y]$ when X and Y are two independent random variables.

Using the properties of Dirac delta functions where required, the expectation values in

Equation 2.24 may be computed as time averages over a finite period in the limit that it goes to infinity. In doing so, we find

$$\begin{aligned}\langle \mathbf{r}(t)\mathbf{r}(t+\tau)\rangle &= \langle r_{A\to B}(t)\rangle\,\delta(\tau) + \langle r_{A\to B}(t)\rangle^2 \\ &\quad - 2\,\langle r_{A\to B}(t)\rangle\,\langle r_{B\to A}(t)\rangle + \langle r_{B\to A}(t)\rangle^2 + \langle r_{B\to A}(t)\rangle\,\delta(\tau) \\ &= \langle r_{A\to B}(t)\rangle\,\delta(\tau) + \langle r_{A\to B}(t)\rangle\,\delta(\tau) + \langle \mathbf{r}(t)\rangle^2 . \end{aligned} \tag{2.25}$$

Inserting Equation 2.25 into Equation 2.21 yields the desired autocorrelation function:

$$R_{\delta\mathbf{r}}(\tau) = \langle r_{A\to B}(t)\rangle\,\delta(\tau) + \langle r_{B\to A}(t)\rangle\,\delta(\tau). \tag{2.26}$$

We may now obtain the power spectral density associated with the fluctuations in $\mathbf{r}(t)$ by substituting $R_{\delta\mathbf{r}}(\tau)$ into Equation 2.4, leading to

$$\begin{aligned} S_{\delta\mathbf{r}}(f) &= 2\int_{-\infty}^{\infty} R_{\delta\mathbf{r}}(\tau)e^{i2\pi f\tau}d\tau \\ &= 2\int_{-\infty}^{\infty} [\langle r_{A\to B}(t)\rangle\,\delta(\tau) + \langle r_{B\to A}(t)\rangle\,\delta(\tau)]e^{i2\pi f\tau}d\tau \\ &= 2\,\langle r_{A\to B}(t)\rangle + 2\,\langle r_{B\to A}(t)\rangle\,, \end{aligned} \tag{2.27}$$

which is seen to have units of $[\mathbf{r}^2(t)/f]$.

In order to obtain the power spectral density associated with the mass-flow fluctuations, we must multiply $S_{\delta\mathbf{r}}(f)$ with the mass of our fluid particles squared. In doing so, we are left with

$$S_{\delta Q}(f) = 2m\,\langle Q_{A\to B}(t)\rangle + 2m\,\langle Q_{B\to A}(t)\rangle\,, \tag{2.28}$$

where we have additionally distributed a factor of m into the averages on the RHS[12], and have defined the quantities $Q_{A\to B}(t)$ and $Q_{A\to B}(t)$ to be the rates of mass flow in the either direction across the pore[13].

Equation 2.28 captures our final result for the power spectral density of the mass-flow fluctuations, and it illuminates the fact that the total noise may be considered as a simple sum of the full shot noises associated with two opposing mass-flow currents across the pore. However, in further development of our analogy with electrical circuits from Chapter 1, we may wish to recast this result in a different form. In particular, we may do so by firstly using the definition of mass conductance from Equation 2.9 to write

$$S_{\delta Q}(f) = 2mGP_A + 2mGP_B, \tag{2.29}$$

where P_A and P_B have been treated as effective pressure differentials across the pore in opposite directions. This is a legitimate maneuver because the particles are statistically independent and the total flow may thus be regarded as the superposition of flows arising from two separate pressure differentials. Refining further, we arrive at the final packaging of our result for the spectral density of mass-flow noise in the free molecular flow regime:

$$\begin{aligned} S_{\delta Q}(f) &= 2mG(\Delta P + P_0) + 2mGP_0 \\ &= 2mG\Delta P + 4mGP_0 \\ &= 2m\left\langle Q(t)\right\rangle + 4k_BTG\rho_0. \end{aligned} \tag{2.30}$$

We note that in the last line of Equation 2.30, the definition of mass conductance has once again been used to make a substitution, with $Q(t)$ being understood as the net rate of mass flow across the pore, *i.e.* $Q(t) = m\mathbf{r}(t)$. We also note that the factor of ρ_0 may be

[12] As discussed in the introduction of this thesis, here the mass m of the fluid particles plays an analogous role to the fundamental unit of charge e in electrical circuits.

[13] The "directions" of these quantities are defined in the same sense as those of $N(t)_{A\to B}$ and $N(t)_{B\to A}$.

regarded as the baseline mass density that exists across both reservoirs in the system and appears after making the appropriate ideal-gas substitution for P_0.

The result as presented in Equation 2.30 lends itself to a straightforward analogy with electrical circuits. Firstly, we note that when $\langle Q(t) \rangle = 0$, or equivalently when the two reservoirs are held at thermodynamic equilibrium, the noise in the system is of strictly thermal origin and may be seen to resemble the result for Johnson-Nyquist thermal noise in electrical resistors. Conversely, when there is no background of randomly moving particles, *i.e.* when $\rho_0 = 0$, the dominant noise in the system is the noise associated with the mean net mass current, $\langle Q(t) \rangle$, and our expression becomes analagous to Shottky's original result for electrical shot noise in vacuum tube diodes.

Motivated by the apparent analogy with electrical circuits, we may choose to identify the first term in our result from Equation 2.30 as the spectral density of *mass-flow shot noise* and the second term as the spectral density of *mass-flow thermal noise*. We may then construct the unitless ratio

$$\frac{\langle (\delta Q_{Thermal})^2 \rangle}{\langle (\delta Q_{Shot})^2 \rangle} = \frac{2P_0}{\Delta P} \tag{2.31}$$

to identify the conditions under which each type of noise is expected to dominate. It may be seen from Equation 2.31 that the thermal fluctuations are dominant when ΔP is small compared with P_0. This is a reasonable expectation because the net flow – which gives rise to the shot noise – will correspondingly be small when compared with the opposing flows resulting from P_0 – which give rise to the thermal noise. Of course, when ΔP is large compared with P_0, it may be seen and indeed expected by the same line of argument that the reverse is true and that the shot noise will dominate. The ratio in Equation 2.31 is plotted below in Figure 2.6 for a range of baseline and differential pressures.

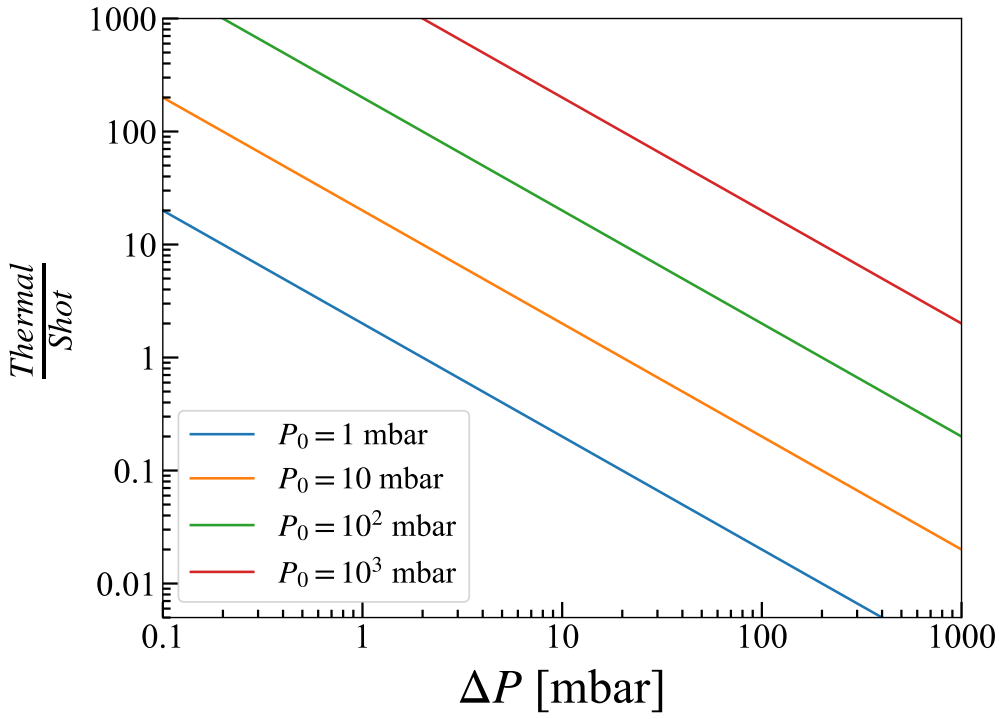

Figure 2.6: The ratio of thermal noise to shot noise plotted against the pressure differential, ΔP, across a cylindrical nanopore. Various baseline pressures, P_0, have been distinguished by line colour. The displayed range of pressures have been somewhat arbitrarily chosen based on typical conditions for free-molecular ^{4}He gas flow in nanopores of ≤ 100 nm diameters. We also reiterate that, strictly speaking, this result is only valid in the free-molecular flow regime.

2.2.4 Additional considerations

We note that our idealization of $\mathbf{r}(t)$ as a series of Dirac delta functions is not realistic for detection in physical systems. The reason for this is that instruments have response times which, in the language of our model, *smear out* the sum of Dirac deltas that we have supposed to constitute $\mathbf{r}(t)$. For instance, in analogy to the measurement of electrical currents, if we consider a detector that counts the amount of mass passing over a point in a time interval of τ seconds, and then divides that count by τ to obtain a measurement of the

mass flow rate, then our detector behaves as a filter with an *impulse response* of

$$h(t) = \begin{cases} \frac{1}{\tau} & |t| \leq \tau/2 \\ 0 & \text{elsewhere} \end{cases}. \tag{2.32}$$

If we suppose that such a detector is used in measuring a one-sided mass current across our pore[14], *i.e.* $Q_{A\to B}$ or $Q_{B\to A}$, then we would expect to see the filtered noise spectrum [11]

$$\begin{aligned} S^{(h)}_{\delta Q_{A\to B}}(f) &= \frac{\sin^2(\pi\tau f)}{(\pi\tau f)^2} S_{\delta Q_{A\to B}}(f) \\ &= \frac{\sin^2(\pi\tau f)}{(\pi\tau f)^2} 2m \left\langle Q_{A\to B}(t) \right\rangle, \end{aligned} \tag{2.33}$$

and likewise for measurements of $Q_{B\to A}$. It is seen from Equation 2.33 that our spectrum is no longer uniform across all frequencies, *i.e.* the noise is no longer *white*, and in particular we note that it diminishes substantially as f approaches and moves beyond $1/\tau$. On the other hand, for frequencies $f \ll 1/\tau$, it is revealed via the small-angle approximation that we recover our original spectrum. Qualitatively, our spectrum would thus become as shown in Figure 2.7.

We also note that in our derivation of mass-flow noise, we have made the implicit assumption that the particles travelling through the nanopore do so instantaneously – or at least with negligible dwell times. It is possible that dwell-time fluctuations will constitute an additional source of noise in the free-molecular flow regime if measurements are performed at a sufficiently high time resolution. In particular, variance in the speeds of incident particles and the random nature of diffuse reflections may contribute to varied transit times across the pore which may manifest as a noise component that has not been considered in the above calculations.

[14] This kind of detector would have to be placed on one side of the nanopore and thus only one component of the flow signal will be measured.

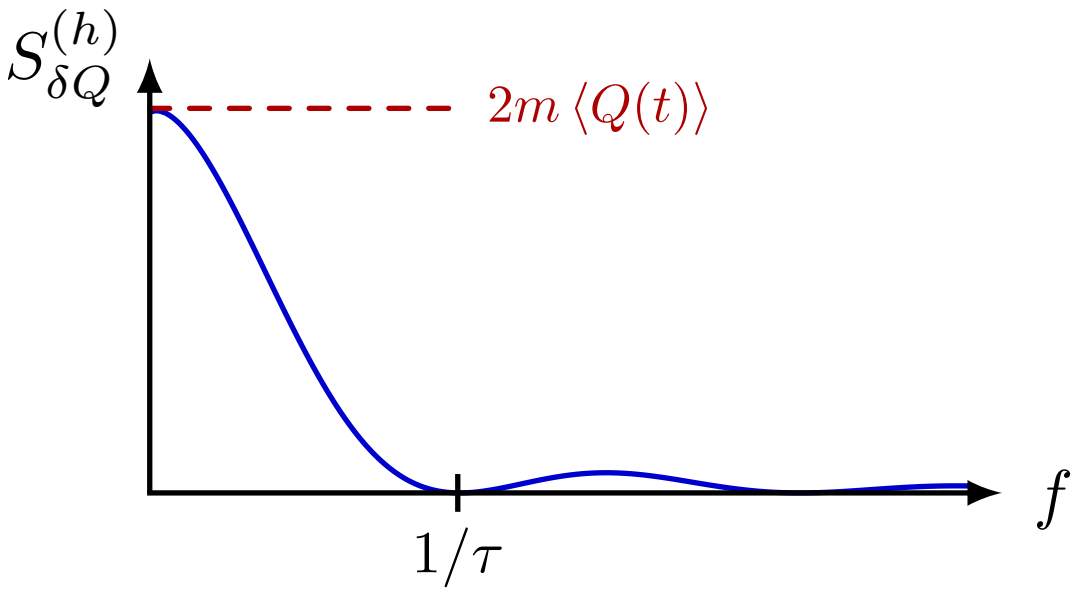

Figure 2.7: Illustration of the frequency dependence of the filtered power spectrum of δQ. It is seen that at low frequencies, *i.e.* those that that justify the use of the small angle approximation in Equation 2.33, the power density is approximately constant with the same value as the original white spectrum. The noise density is also seen to fall off dramatically as the frequency approaches (and moves beyond) values that are comparable with $1/\tau$.

Finally, we have also neglected any consideration of surface effects. Since the dominant scattering mechanism inside of the free-molecular regime is collisions with the wall, there is a possibility that surface effects may play some appreciable role in determining the behaviour of gas flow, particularly in long pores where more collisions are expected to take place. For short pores, where the number of collisions is expected to be small, it may be more appropriate to neglect such surface effects.

2.3 Simulations of free-molecular flow

The simulations presented in this thesis consist in two parts: firstly, we estimate the transmission probabilities – *i.e.* the Clausing factors – of particles passing through nanopores of varying geometries. This is done using a modified version of the Monte Carlo program that was written by a previous member of GervaisLab [15]. The results here obtained are then used as a proxy for the prediction of free-molecular conductance in nanopores.

Secondly, we expand on this basic Monte Carlo infrastructure by tracking the particles through time. In doing so, we rig our program with the ability to simulate a fluctuating flow signal from which we may extract a measure of simulated mass-flow noise in the free-molecular regime.

2.3.1 Monte Carlo estimation of the Clausing factor in nanopores

Monte Carlo methods (or *simulations*) refer to a broad class of numerical strategies for estimating properties of a process that has been modelled probabilistically. The basic anatomy of a Monte Carlo program consists of repeated, randomly-seeded initializations of some deterministic computation. The result of the method is generally to yield some desired statistical measure of the process under study.

In the previous section, we have developed a stochastic model for free-molecular flow through nanopores. This we have done in the language of randomized particle trajectories and their statistics, which together comprise a probabilistic picture of the gas flow. The Monte Carlo method of simulation is thus quite naturally suggested, and, in particular, the assumed statistical independence of particles in our model entitles us to use the *test-particle* method.

Specifically, our simulation is comprised of a collection of repeated, independent trials which begin with a test particle that is initialized with a random position at the entrance of the nanopore. From this point, a randomized trajectory is assigned and a set of path lengths

are computed to determine whether the particle will successfully transmit, collide with the wall, or get reflected back out of the entrance of the pore. The structure of the test-particle method here employed is illustrated below in Figure 2.8.

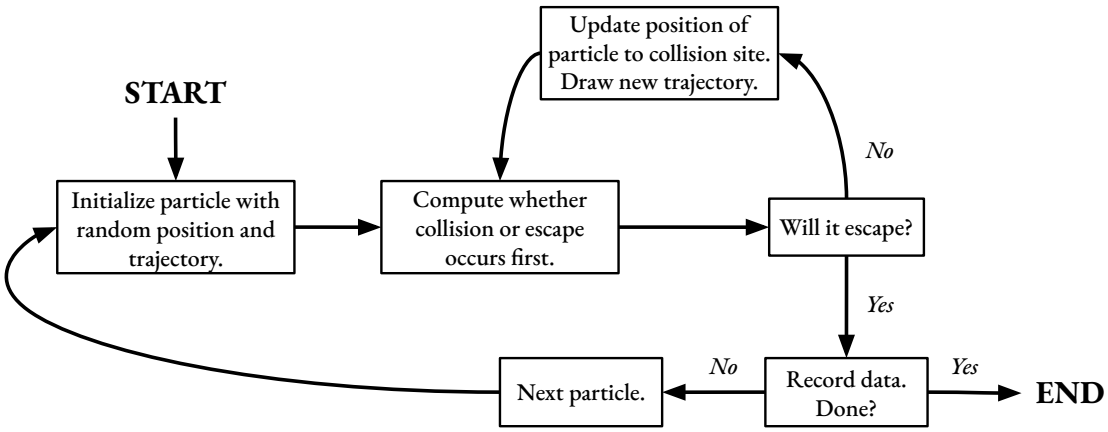

Figure 2.8: Flow chart that captures the basic steps involved in the test-particle Monte Carlo program for estimating the transmission probabilities of particles through the nanopore.

We note that two versions of the simulation are developed: one for cylindrical nanopores and one for conical nanopores. The L/R ratio of the nanopore may be tuned in both versions, while the opening angle may also be tuned in the conical case. We additionally note that, as is conventional for the simulation of rarefied gases [16, 17], collisions with walls are assumed to be diffuse. This means that the random particle trajectories at each step (including initialization) may be sampled from the cosine law distribution, *i.e.* from

$$f_{\theta,\phi}(\theta,\phi) = \frac{1}{\pi}\cos(\theta)\sin(\theta). \tag{2.34}$$

Equation 2.34 implies that each angle may be independently selected under the corresponding probability density functions

$$f_{\theta}(\theta) = 2\sin(\theta)\cos(\theta) = \sin(2\theta) \tag{2.35}$$

and

$$f_\phi(\phi) = \frac{1}{2\pi}. \tag{2.36}$$

A basic implementation of parallel processing in Python is used to run multiple instances of the above-described trials simultaneously. Once all the computations are finished, the aggregate results for transmission and reflection counts are used to estimate the transmission probability of particles incident on the surface of the pore. A set of results for differing pore geometries is presented in Figure 2.9.

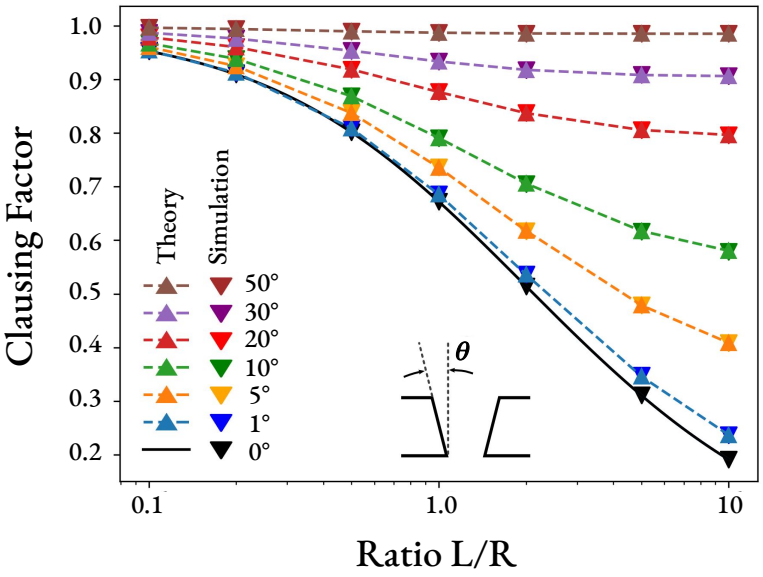

Figure 2.9: Comparison of Clausing factors extracted from the simulation with values that have been previously computed via theoretical methods [18]. Note that the theoretical values contained in the figure were computed and tabulated for a discrete set of L/R and θ values, which are plotted with upward triangles, and that the dashed lines represent simple linear interpolations through these points. The solid black line corresponding to $\theta = 0$ is the exception, as the theoretical result in this case is a closed-form expression of L/R.

The simulation of Clausing factors by this method may prove useful for modelling the conductance of nanopores in the free-molecular flow regime. The connection comes from

Equation 2.12 and Equation 2.13, which together lead us to the expression

$$\begin{aligned}\langle Q_{A\to B}(t)\rangle &= m\,\langle r_{A\to B}(t)\rangle \\ &= m\kappa_{A\to B}\,\langle r_A(t)\rangle \\ &= \Bigg(\underbrace{\kappa_{A\to B}\frac{1}{4}\sqrt{\frac{m\pi}{2k_BT}}D^2}_{G}\Bigg)P_A \end{aligned} \tag{2.37}$$

where we have identified the free-molecular conductance G by again treating P_A as an effective pressure differential across the pore – and thus by referring to Equation 2.9.

It may be seen explicitly from Equation 2.37 that our simulated Clausing factors may indeed be used as a proxy for estimating the mass conductance of nanopores in the free-molecular flow regime. As a proof of concept, the simulation was used to predict the free-molecular conductances for a collection of pores that have been previously characterized by members of GervaisLab. Images of the pores are contained in Figure 2.10 and Table 2.2 summarizes the results of the simulations.

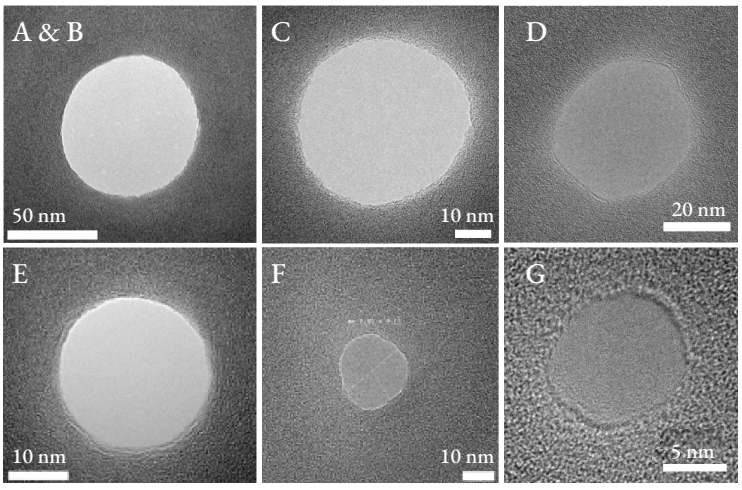

Figure 2.10: Top-down images taken of the nanopores under study. The images were taken using a transmission electron microscope (TEM) by M. Savard (pores A-F) and P.-F. Duc (pore G) [13, 19].

Label	R (nm)	L (nm)	Opening Angle	Temp. (K)	G_{exp} (nm·ns)	G_{sim} (nm·ns)
A	38.5	50	11°	77	3.78	3.58
B	38.5	50	11°	295	1.91	1.83
C	23.3	50	12°	295	0.627	0.638
D	20.5	50	5.0°	77	0.893	0.769
E	12.5	75	5.0°	77	0.115	0.224
F	10.6	30	7.0°	77	0.191	0.213
G	3.06	30	15°	77	0.207	0.207

Table 2.2: Simulated conductance results (with $N_{\text{particles}} = 2000000$) corresponding to each of the labelled pores. The experimental conductances that were obtained by M. Savard and P.-F. Duc may also be found in the table for comparison [13, 19]. Note that the R measurements were predominantly made using TEM imaging of the pores under study, but occasionally new measurements were taken in situ by the fitting of the measured gas flow – this was done to account for the fact that the pores, particularly the smaller ones, had a tendency to shrink over time. All quoted opening angles for the nanopores were found via modelling as well; more details may be found in the referenced theses.

2.3.2 Simulation of the stochastic flow signal

An instantaneous flow signal may be simulated using an extension of the Monte Carlo method employed above, which we here demonstrate using a simple cylindrical pore geometry. In order to do so, we once again model the particle arrivals at the entrance of the pore as a Poisson process and generate a collection of arrival times in accordance with Equation 2.8. This is done using a tau-leaping procedure with propensities from Equation 2.12. Initialized particles are now indexed by their times of arrival at the nanopore entrance and additionally receive a randomly-assigned speed in accordance with the distribution

$$f(v) = \frac{1}{2}\left(\frac{m}{k_B T}\right)^2 v^3 e^{-mv^2/2k_B T}, \tag{2.38}$$

which may be understood as the ordinary Maxwell-Boltzmann distribution after being skewed toward higher speeds[15]. As the computations are executed, the time spent inside the pore

[15]This to account for the fact that faster particles reach the pore more often.

is tracked for each particle and, for successfully transmitted particles, the resultant lag is added to its initial arrival time to yield a transmission time. The total count of particle transmissions as a function of time, *i.e.* $\mathbf{N}(t)$, may then be constructed as shown in Figure 2.11 for a set of L/R ratios and temperatures.

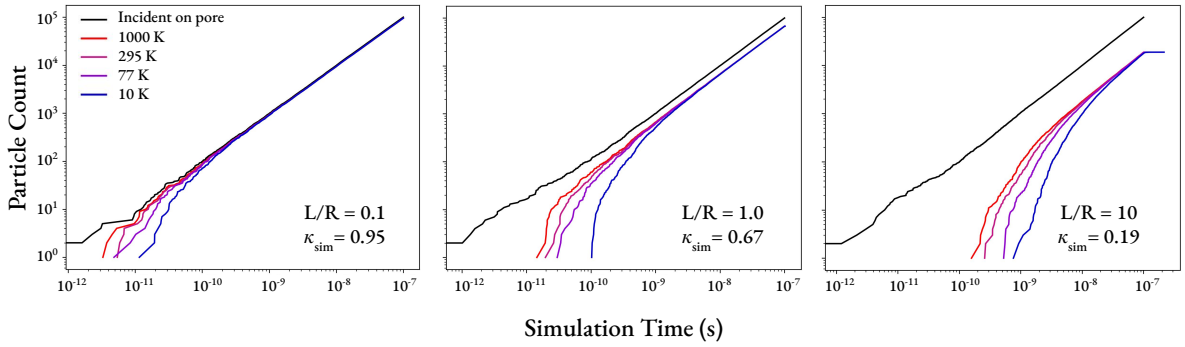

Figure 2.11: Simulated count of particle transmissions through cylindrical nanopores over a simulated time period of roughly 10^{-7} seconds. The rate parameter for particles arriving at the entrance of the pore is held constant at $\langle r_A \rangle = 10^{12}$ particles per second, with the total number of arrivals accumulated tracked in black. The coloured plots correspond to the counts of particle transmissions for a range of temperatures. The L/R ratio varies across simulations and a simulated Clausing factor κ_{sim} is extracted from each simulation by dividing the particle transmission count by the count of incident particles at the end of the run. The radius of the simulated nanopore is fixed at the somewhat arbitrary choice $R = 30$ nm. Note that the vertical axes are aligned across all three plots.

Once the count of particles through time has been simulated, we may choose a time step τ over which to compute an average rate of flow and construct our fluctuating flow signal – this being done in analogy to Equation 2.32. Converting the plots from Figure 2.11 into time traces of the flow rates using $\tau = 10^{-10}$ seconds gives what is shown in Figure 2.12. Note that the results presented here may be interpreted as d.c. images of the underlying c.c. (simulated) flow rates, which give rise to the simulated step functions from Figure 2.11.

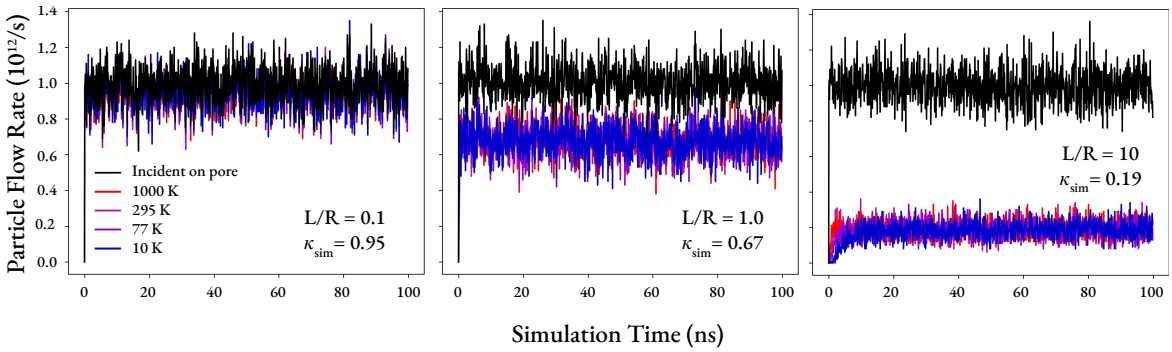

Figure 2.12: Time traces of particle flow rates extracted from the simulation results presented in Figure 2.12. The time step used for averaging is $\tau = 10^{-10}$ seconds. The obtained flow rates are positioned in time at the centers of their averaging windows, such that each simulated data point is separated by a period of $\tau/2 + \tau/2 = \tau$.

2.3.3 Analysis of the simulated flow noise

Our simulation measures the rate of mass flow by averaging over periods of $\tau = 10^{-10}$ seconds. The noise that we should expect to see is thus reflected in the filtered spectrum defined in Equation 2.33 under the appropriate substitutions. The total power of the fluctuations delivered to the simulation is thus

$$\langle (\delta Q_\tau)^2 \rangle = 2m \langle Q(t) \rangle \int_0^\infty \frac{\sin^2(\pi\tau f)}{(\pi\tau f)^2} df,$$

where we have subscripted δQ_τ with τ to distinguish it from the idealized, non-averaged fluctuations in $Q(t)$. The integral may be solved by differentiating under the integral sign

twice. Namely, we start with

$$\begin{aligned} g(\alpha) &= \frac{2m\langle Q(t)\rangle}{\pi\tau}\int_0^\infty \frac{\sin^2(\alpha u)}{u^2}e^{-\beta u}du \\ \rightarrow g'(\alpha) &= \frac{2m\langle Q(t)\rangle}{\pi\tau}\int_0^\infty \frac{\partial}{\partial\alpha}\frac{\sin^2(\alpha u)}{u^2}du \\ &= \frac{2m\langle Q(t)\rangle}{\pi\tau}\int_0^\infty \frac{2\sin(\alpha u)\cos(\alpha u)}{u}du \\ &= \frac{2m\langle Q(t)\rangle}{\pi\tau}\int_0^\infty \frac{\sin(2\alpha u)}{u}du, \end{aligned} \tag{2.39}$$

where we have initialized the calculation with a u-subsitution. For the second differentiation, we may write

$$\begin{aligned} z(\beta) &= \frac{2m\langle Q(t)\rangle}{\pi\tau}\int_0^\infty \frac{\sin(2\alpha u)}{u}e^{-\beta u}du \\ \rightarrow z'(\beta) &= \frac{2m\langle Q(t)\rangle}{\pi\tau}\int_0^\infty \frac{\partial}{\partial\beta}\frac{\sin(2\alpha u)}{u}e^{-\beta u}du \\ &= -\frac{2m\langle Q(t)\rangle}{\pi\tau}\int_0^\infty \sin(2\alpha u)e^{-\beta u}du, \end{aligned} \tag{2.40}$$

where the integral in the last line may be solved via repeated integration by parts. The result is then straightforwardly integrated with respect to β, yielding

$$z(\beta) = -\frac{2m\langle Q(t)\rangle}{\pi\tau}[\tan^{-1}(\beta/2\alpha) + C] \tag{2.41}$$

where the constant of integration may be found by noting that the limit of $z(\beta)$ as β goes to infinity must equal zero. This implies that $C = -\pi/2$ and thus we have

$$z(0) = \frac{m\langle Q(t)\rangle}{\tau}, \tag{2.42}$$

which may be integrated with respect to α to obtain

$$g(\alpha) = \frac{m\langle Q(t)\rangle}{\tau}\alpha + C', \tag{2.43}$$

with C' such that $g(0) = 0$. Finally, we substitute $\alpha = 1$ to arrive at our result for the expected simulation noise,

$$\langle(\delta Q_\tau)^2\rangle = \frac{m\langle Q(t)\rangle}{\tau}. \tag{2.44}$$

Note that the result above carries with it the implicit assumption that dwell times in the pore are negligible. For this reason, we now consider a simplified version of the simulation in which the particle transmissions occur instantaneously. We also note that $\langle Q(t)\rangle$ may be replaced with $\kappa\langle r_A\rangle$ in Equation 2.44, with κ taken from the theory equation that was plotted previously in Figure 2.9 for cylindrical nanopores. For each simulation, the simulated noise is calculated as the mean square fluctuation of the simulated flow signal and converted to mass-flow noise via multiplication with m^2. Comparisons between the theoretical predictions and the results from the simulation are presented in Table 2.3 below.

L/R	κ	Theory Noise (10^{-31} kg^2/s^2)	Sim. Noise (10^{-31} kg^2/s^2)
0.1	0.95239890732	4.20727976	4.25573590
0.5	0.80127142718	3.53966498	3.48949246
1.0	0.67198412851	2.96853052	2.99412614
5.0	0.31053455381	1.37180517	1.37475242
10	0.19099354799	0.84372554	0.82618460

Table 2.3: Total noise powers contained in a set of simulated mass-flow signals and the corresponding noise powers expected to be seen from theory. The presented simulation results are averages across 10 runs, with each run simulating a period of 10^{-7} seconds. Once again, the rate of particle arrivals at the entrance of the pore is held constant at $\langle r_A\rangle = 10^{12}$ particles per second.

Chapter 3

Preliminary experiments

3.1 Method

In this section, we outline the method used in conducting preliminary experiments aimed toward the detection and characterization of mass-flow noise in the free-molecular flow regime. Specifically, we describe our first attempts at detecting fluctuations in dilute helium-gas flow inside a simple nanopore system having $P_A = \Delta P$ and $P_B \approx 0$. The experiments discussed here are not intended to represent a finalized procedure for measuring mass-flow noise in the free-molecular regime, but rather function as the initialization of a basic approach that is in need of further refinement.

3.1.1 Aim and strategy

The purpose of these experiments is broadly to establish the beginnings of a noise measurement scheme to be used in the study of flow noise in nanopore systems. Our investigations are motivated by the results obtained in the theory and simulation sections of this thesis, which have been put forth as measures of the limiting behaviour we should expect to see.

We set out in our pursuit with the strategy of detecting the mass-flow shot noise as-

sociated with a simple free-molecular fluidic system in which a nanopore is put between a reservoir of a dilute gas and a vacuum. The gas used in these experiments is helium-4, which is the most inert and relatively easy to detect using a mass spectrometer, thus making it an ideal candidate. It is expected that the fluctuations in flow rate reported from the mass spectrometer should be comparable to the theoretical noise expressions found previously for the free-molecular flow regime.

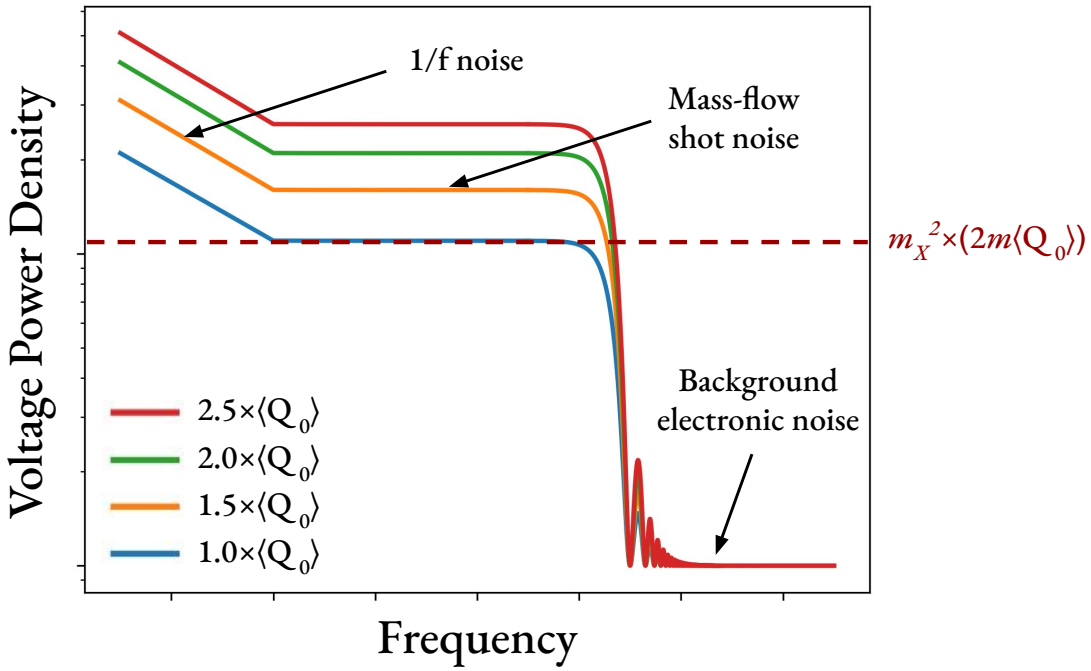

Figure 3.1: Cartoon (log-log) plot of what behaviour we may expect to see in the power spectrum of a voltage output proportional to Q. In particular, there is a $1/f$ component depicted at low frequencies which is a typical feature of noise in measurement systems [20] and which is seen to eventually fall off into a flat region of the spectrum. We may also expect to observe a flat frequency band corresponding to the anticipated mass-flow shot noise expression from the previous chapter. The subsequent drop off is expected based on the necessarily finite response time of our measurement instrument, which should dampen the mass-flow fluctuations around some cut-off frequency. In higher frequencies, all that is left is any background noise that is independent of the signal fed into the system. Note that the scaling of the mass-flow noise expected to be seen in the flat region is illustrated for factors ranging from 1 to 2.5 times some initial flow Q_0 of mean $\langle Q_0 \rangle$. If the conversion process between the mass flow and the voltage output is done uniformly across all frequencies, then – neglecting other sources of noise – the expected power density would be $m_X^2 \times (2m\,\langle Q \rangle)$, with m_X representing the conversion factor in units of [voltage/mass flow] and being named in such a way so as to foreshadow the characterization that is done in 3.2.2.

Given that measurements of the flow will be obtained from a mass spectrometer as a voltage signal, our initial expectations for what is expected to be observed may be summarized in more detail via Figure 3.1. Of course, this figure gives only a simplified and largely qualitative picture of what we might expect to see; in reality, it is expected that we should have to contend with additional complications and sources of noise in order to extract a genuine measure of the mass-flow fluctuations.

3.1.2 Experimental setup

The setup used in conducting these noise experiments has much overlap with those used by past GervaisLab members and indeed recycles many of their components [13, 19, 21, 22]. Firstly, a nanopore is held in a stainless steel cell which is connected to a gas control panel, allowing for the the pressure differential across the pore to be incremented in small steps. The bottom of the pore is then maintained at high vacuum and connected to a Pfeiffer Vacuum HLT-560 Helium Leak Detector for the detection of the transmitted helium atoms.

Since the HLT-560 outputs averages of the signal at a rate of 20 Hz, we located and intercepted the signal at an earlier stage in an attempt to measure with a higher time resolution, *i.e.* lower τ in Equation 2.32. This was done via direct connection to the electrometer amplifier unit (the EVV) inside the instrument, which converts the current from the Faraday cup inside the mass spectrometer into a voltage signal at four possible levels of amplification[1]. Measurements of the noise are obtained by feeding the voltage signal from the electrometer amplifier unit of the HLT-560 to a Stanford Research SR830 lock-in amplifier. The noise at a range of discrete frequencies is estimated via calculation of the mean average deviation (MAD), which is done internally by the lock-in amplifier. A diagram of the setup is provided below in Figure 3.2.

[1] There is no mention of any quantitative details on these amplification settings in the instrument manuals.

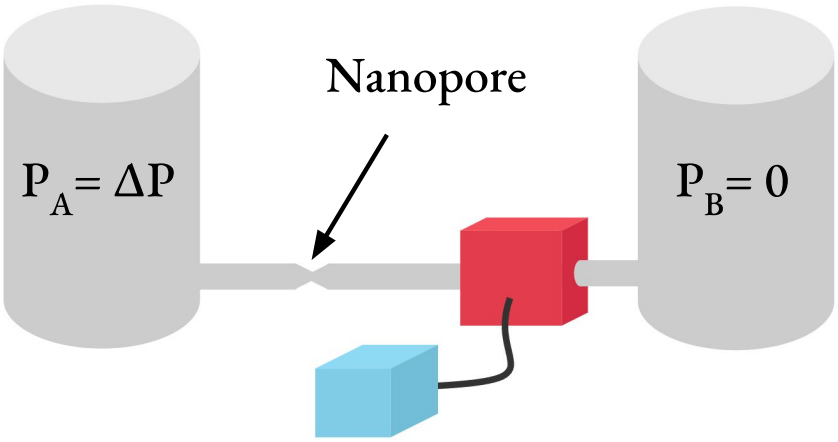

Figure 3.2: Cartoon of the experimental setup. The red cube represents the HLT-560 leak detector while the blue cube represents the SR830 lock-in amplifier.

3.2 Results

3.2.1 Characterization of the nanopore

All nanopores used in these experiments were drilled into silicon nitride membranes using a scanning electron microscope, as was done in the previously-referenced GervaisLab work. The particular nanopore used for the results presented in this thesis was drilled with an effective radius $R = 40.8$ nm in a membrane of thickness $L = 30$ nm. The pore was characterized by its experimental conductance in the free-molecular flow regime over a range of appropriate pressures. The result as a function of Kn is presented in Figure 3.3 alongside a TEM image of the pore which was taken at the time of fabrication. Running our simulation using the average conductance measured in the free-molecular regime, $G_{exp} = 2.38$ nm·ns, and the quoted dimensions of the pore yields an estimated opening angle of approximately $\theta \approx 20°$.

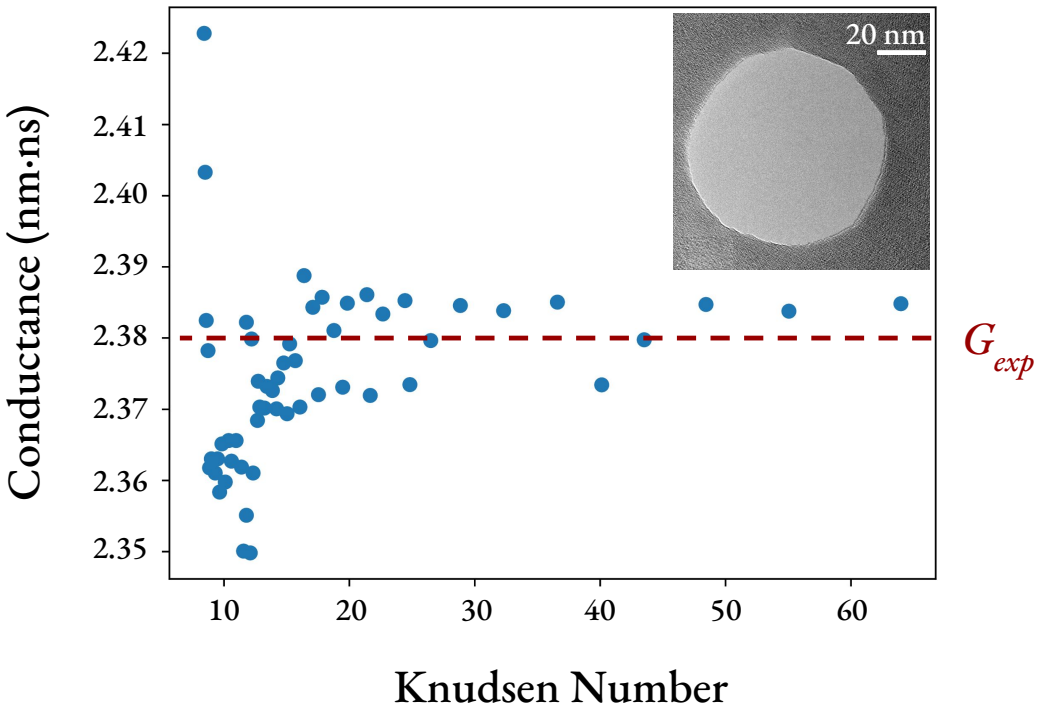

Figure 3.3: Plot of experimental conductance vs Knudsen number. We note that it is expected from past work that the conductance will depart from the free-molecular value as the Knudsen number approaches and moves below 10. Specifically, it is expected and indeed here shown that the conductance should begin to increase rapidly as we depart from the free-molecular regime near Kn = 10. Taking the average of the conductance values measured for Kn > 15 gives approximately $G_{exp} = 2.38$ nm·ns. Credit goes to undergraduate student Julien Hacot-Slonosky for taking the data shown here.

3.2.2 Characterization of the electrometer amplifier unit

As mentioned above, noise measurements were taken directly from the electrometer amplifier unit. This was done in an attempt to avoid the restrictive averaging that occurs inside the processing electronics of the HLT-560. Very little information was available on the specifications of the electrometer amplifier unit aside from the fact that it converts a current into an amplified voltage signal that is then passed to the internal electronics of the leak detector. Details on the precise conversion factors, amplification settings, response time, etc. of the this device were not available directly. In order to proceed, it was thus necessary to firstly identify the wire that carries the signal of interest and to then characterize, experimentally, the effective conversion rates between the measure of mass flow (in units of kg/s) and the

output voltage.

In particular, for our investigations we focused on relatively low pressure differentials in order to remain in the free-molecular regime, and consequently only encountered two of the four quoted amplification settings. The results for a basic characterization of each setting is contained in Figure 3.4.

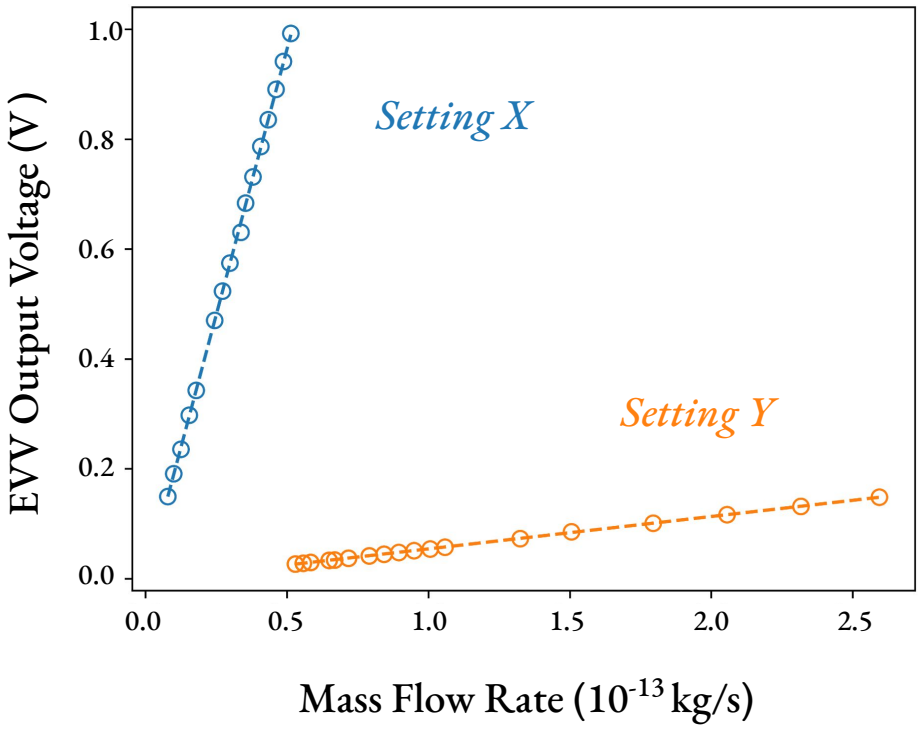

Figure 3.4: Characterization of the two amplification settings encountered during these experiments, which we have here dubbed *Setting X* and *Setting Y*. For Setting X and Setting Y respectively, the linear fits characterize conversion rates of $m_X = 1.94 \times 10^{16}$ mV·s/kg and $m_Y = 5.90 \times 10^{14}$ mV·s/kg (with offsets of $b_X = -6.10$ mV and $b_Y = -5.17$ mV).

3.2.3 Noise observations

Our aim in this subsection is to provide a brief summary of the salient, qualitative features that were observed and several-times reproduced during these noise experiments. We adopt this modest goal in concession to the fact the HLT-560 was in many ways operating outside the scope of the information that was available to us. This lack of understanding – with respect to qualities such as the gain profile of the amplifier and its inherent noise

characteristics – made most quantitative interpretations of the data unreliable at this stage of the experiments, particularly in the respect of confirming the expected mass-flow noise from our previous analyses.

Figure 3.5 contains plots of two noise measurements taken at sequential flow rates in Setting X of the amplifier[2]. The results presented in this figure are emblematic of the main qualitative properties of the electrometer amplifier noise that were observed over the course of our investigations. Namely, it is seen that the noise spectra are approximately flat in the 1-5 Hz frequency band and fall off dramatically as the frequency approaches and moves beyond the quoted measurement speed of the HLT-560. In addition, a series of measurements across six different flow rates found that the average noise density over the 1-5 Hz band was fitted relatively well against the average rate of mass flow with a straight line. This appears to indicate that the total noise within the flat region of the spectra is approximately proportional to the corresponding average mass flow rates, however more data would be needed to say so definitively – and especially needed in order to say whether this suspected proportionality is indeed an artifact of innate fluctuations in the mass flow or rather of something else.

It should also be noted that occasionally strange behaviour was observed in collected data. For instance, sometimes sharp peaks would appear and the noise seen would increase dramatically. Most commonly, this kind of behaviour occurred when dealing with lower flow rates well into the free-molecular regime. It is advised that future measurements be done multiple-times over to ensure that they are reproducible, and that investigations be conducted especially into the behaviour of the measured spectra for very low flow rates (*e.g.* $\lesssim 10^{-8}$ mbar·l/s[3]).

[2]Setting Y is typically only activated for flows well outside the free-molecular regime. As such, most of the noise experiments were done inside of Setting X by virtue of our confinement to high Kn.

[3]These are units of *energy* flow, namely those in which the HLT-560 reports its measurements by default. Conversion to mass flow may be done using the ideal gas law.

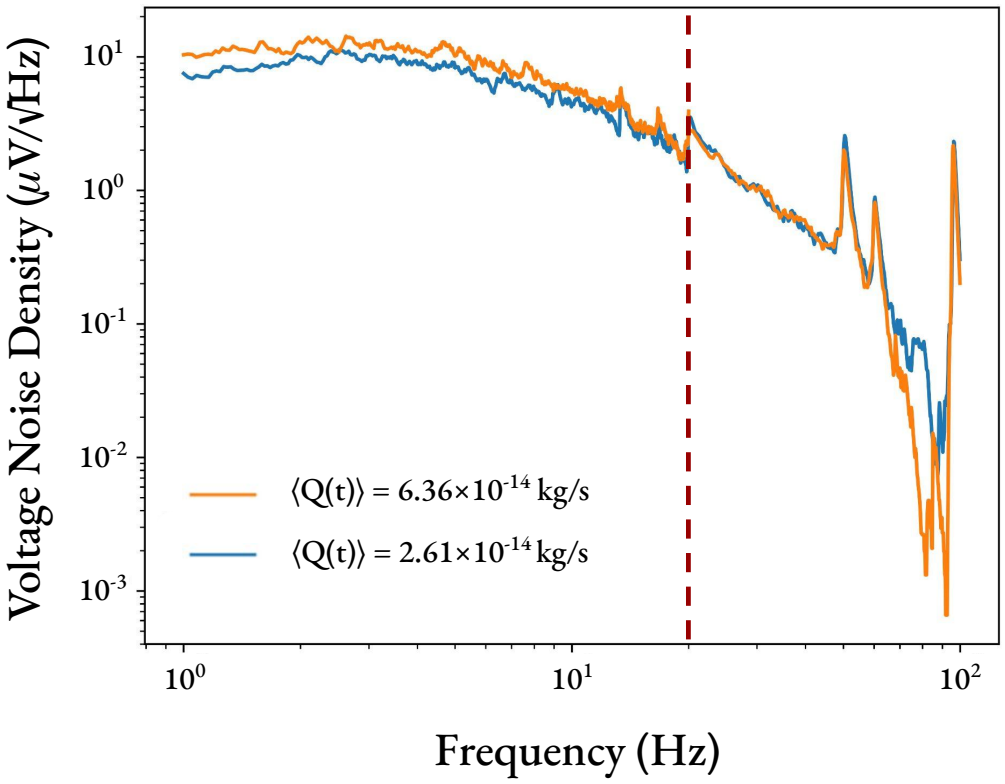

Figure 3.5: Plots of two noise measurement runs over the frequency band 1-100 Hz. The data was taken using the same nanopore that is characterized in Figure 3.3. Note that there appears to be a relatively flat region in the spectra near low frequencies which falls off significantly around the quoted measurement rate of the HLT-560, *i.e.* 20 Hz (shown in the figure with a red dashed line). The plots are also suggestive of a correlation between the noise density at low frequencies and the average mass flow rate. Note however that, based on what was shown in Figure 3.1, we were expecting to measure noise densities equal to $m_X\sqrt{2m\langle Q\rangle}$ in the approximately flat region, which in this case equals about 0.36 $\mu\text{V}/\sqrt{\text{Hz}}$ and 0.56 $\mu\text{V}/\sqrt{\text{Hz}}$ for the lower and higher flow signals respectively. The discrepancy between these expected values and what is seen here (roughly an order of magnitude) is not currently understood.

Chapter 4

Conclusion and outlook

4.1 Conclusion

In this thesis, we have provided a foundation for studying fluctuations and noise in small-scale, gaseous fluidic systems. We have called upon various analogies from theoretical work that has been done for electrical circuits, and in this sense have played the modest role of extending such manners of thought into a new realm for which they appear to be also applicable.

The first stream of anlaysis that we have done in this respect has been theoretical. Following in the footsteps of previous work on electrical fluctuations, we have derived the power spectral densities associated with the limiting mass-flow fluctuations proposed to exist in a simple class of free-molecular fluidic systems. We have identified these fluctuations as the sum of two full shot noises associated with statistically independent mass-flow currents in either direction across the pore. In further development of our analogy with electrical circuits, we have also seen that such fluctuations may be split into so-called *mass-flow thermal noise* and *mass-flow shot noise* contributions, with proportions governed by the unitless ratio $2P_0/\Delta P$. In addition, we have mentioned certain complicating factors that may relate to future experimental work, such as the effects of filtering and the unaccounted-for surface

effects and variance in dwell times.

We have also given an account of a Monte Carlo program that has been used to estimate transmission probabilities of particles through pores and rigged with the ability to simulate time traces of a fluctuating flow signal. The simulation was used to estimate Clausing factors in a variety of pore geometries and was found to agree with theoretical results from past work. The utility of such a program in serving as a proxy for simulating nanopore conductances in the free-molecular regime is also discussed. Additionally, the power of the fluctuations present in the simulated flow signals were calculated and found to agree very well with our prior theoretical analysis.

Finally, we have loosely documented the beginnings of an experimental effort to study the inherent fluctuations that exist in free-molecular flow through nanopores. The results of these preliminary experiments do not permit us to make any definitive claims about this central object of our study, but do however reveal certain features of our measurement apparatus which may be useful in calibrating what are the prudent next steps in this direction.

4.2 Outlook

The work presented in this thesis is expected to serve as a foundation for pursuing further experimental work in measuring and characterizing fluctuations in gaseous fluidic systems, especially in the free-molecular regime. Explicitly, it may be possible to deploy both the theoretical and computational platforms established here to guide such measurements in the future, whether by technical means similar to those undertaken in the described preliminary experiments or by others which may be more ideal for this purpose.

For instance, in further development of the method outlined in the previous chapter, it would be useful to optimize the procedure to characterize the voltage noise spectra for an extended sequence of increasing flow rates. In addition, measurements should be taken to establish a reliable background which may be subtracted from subsequent data so that

what is dealt with is strictly the change in the spectra that is affected by the varying of the average flow rate. Once the relationship between $\langle Q(t) \rangle$ and the observed noise has been more thoroughly and reliably quantified, a comparison with theoretical expectations, *i.e.* vis-à-vis the contents of Figure 3.1, may be better made. Considering the large discrepancy that currently seems to exist in this respect, which is detailed in the caption of Figure 3.5, it may turn out that additional noise sources are indeed corrupting the band where we expected to see the mass-flow fluctuations, and thus it may also be important to begin considering other noise sources in the system. In particular, it may be the case that there exists additional noise that is proportional to either $\langle Q(t) \rangle$ or $\langle V(t) \rangle$, which may render it difficult to assess where any observed proportionalities originate from. Note that in dealing with such excess noise, it may be useful to deliberately extend measurements made to beyond the free-molecular regime. This would be done in the hope that the expected positive linear relationship between the mass-flow noise power and the average flow rate will diminish as the signal becomes more correlated with itself by virtue of the onset of inter-particle collisions (*i.e.* entrance to the continuum regime). It might be possible to extract a measure of the mass-flow fluctuations from considerations along this line.

Otherwise, if a new measurement system is built from components for which the various crucial technical characteristics are known or can in principle be easily uncovered, then the observed fluctuations and noise profiles may be more readily interpreted and navigated, such that a quantitative measure of the inherent mass-flow fluctuations may be made on firmer ground. For this purpose, details such as the gain profiles and inherent noise characteristics of amplifiers and other electronics used would be especially important to have. In addition, it is expected that a detector operating with a higher resolution in time would widen the bandwidth of mass-flow fluctuations that make it through to the measurement output. This could make such fluctuations much easier to see. We also note that by having clarity on the operation of the instruments used, it may be possible to filter the signal into a suitable band for which the expected noise power may be calculated from theory or simulation and then

compared with the results of experiment.

It is also expected that once the facility for dealing with mass-flow signals on such small scales has been properly built, both insofar as its resolution in time as well as in its magnitude, then it may be possible to undertake much more sensitive experimental projects. In other words, it is possible that future technologies or investigations in nanopore systems may be contingent on an understanding of these more delicate features of the mass flow.

Finally, we note that it may be possible to use the simulation to inject complications into our analysis of mass flow. For instance, it may be possible to add intermittent, temporary blockades to the pore which alter the Monte Carlo algorithm for some finite period of time. This may give some insight into how such blockades impact the time structure of the signal and at what scales. In addition, the effects of asymmetry in pores, for instance pores with some geometrical defects, may be studied using some modified version of the simulation as well – either in terms of the expected character of fluctuations or in terms of the manifest Clausing factors.

References

[1] D. Abbott, Overview: unsolved problems of noise and fluctuations, *Chaos: Interdisc. J. Nonlinear Sci.* **11**, 526 (2001).

[2] J. B. Johnson, Thermal agitation of electricity in conductors, *Phys. Rev.* **32**(1), 97-109 (1928).

[3] H. Nyquist, Thermal agitation of electric charge in conductors, *Phys. Rev.* **32**(1), 110-113 (1928).

[4] W. Schottky, Über spontane stromschwankungen in verschiedenen elektrizitätsleitern, *Ann. Phys. (Leipzig)* **362**(23), 541–567 (1918).

[5] C. Wen and S.-L. Zhang, Fundamentals and potentials of solid-state nanopores: a review, *J. Phys. Appl. Phys.* **54**, 023001 (2021).

[6] Y. Wang, Y. Zhao, A. Bollas, Y. Wang, and K. F. Au, Nanopore sequencing technology, bioinformatics and applications, *Nat. Biotechnol.* **39**, 1348-1365 (2021).

[7] M. Savard, C. Tremblay-Darveau, and G. Gervais, Flow conductance of a single nanohole, *Phys. Rev. Lett.* **103**, 104502 (2009).

[8] J. Dastoor, D. M. Willerton, W. Reisner, and G. Gervais, Noise and fluctuations in nanoscale gas flow, *Phys. Scr.* **98**, 075013 (2023).

[9] A. Papoulis, S. U. Pillai, *Probability, Random Variables, and Stochastic Processes* (4th ed.) (McGraw Hill, 2002).

[10] W. C. van Etten, *Introduction to Random Signals and Noise* (John Wiley & Sons, Inc., 2005)

[11] R. D. Yates, *Probability and Stochastic Processes* (2nd ed.) (John Wiley & Sons, Inc., 2005).

[12] S. Engelberg, *Random Signals and Noise: A Mathematical Introduction* (CRC Press, 2007).

[13] M. Savard, Mass transport in single nanopores, Ph.D. thesis, McGill University (2014).

[14] T. T. Heikkilä, *The Physics of Nanoelectronics: Transport and Fluctuation Phenomena at Low Temperatures* (Oxford University Press, 2013).

[15] D. Crook, Simulation of gaseous mass flow through nanopores with Monte Carlo methods, Undergraduate thesis, McGill University (2021).

[16] W. Steckelmacher, Knudsen flow 75 years on: the current state of the art for flow of rarefied gases in tubes and systems, *Rep. Prog. Phys.* **49**, 1083 (1986).

[17] J. Gómez-Goñi and P. J. Lobo, Comparison between Monte Carlo and analytical calculation of the conductance of cylindrical and conical tubes, *J. Vac. Sci. Technol. A 21*, 1452-1457 (2003).

[18] P. Clausing, The flow of highly rarefied gases through tubes of arbitrary length, *J. Vac. Sci. Technol.* **8**(5), 636–646 (1971).

[19] P.-F. Duc, Quasi–one-dimensional superfluidity, Ph.D. thesis, McGill University (2018).

[20] F. N. Hooge, Experimental studies on 1/f noise, *Rep. Prog. Phys* **44**, 479 (1981).

[21] G. Dauphinais, Fabrication, structural relaxation, and flow in solid-state nanopores, M.Sc. thesis, McGill University (2012).

[22] S. Neale, High speed flow through silicon nitride nanopores as a potential dumb hole, Ph.D. thesis, McGill University (2013).